In Situ Raman Probing of Graphene over a Broad Doping Range upon Rubidium Vapor Exposure

Romain Parret,[†] Matthieu Paillet, Jean-Roch Huntzinger, Denise Nakabayashi,[⊥] Thierry Michel, Antoine Tiberj, Jean-Louis Sauvajol, and Ahmed A. Zahab*

Laboratoire Charles Coulomb UMR 5221, Université Montpellier 2, F-34095 Montpellier, France and CNRS, Laboratoire Charles Coulomb UMR 5221, F-34095 Montpellier, France. [†]Present address: Laboratoire Pierre Aigrain, Ecole Normale Supérieure de Paris, 24 Rue Lhomond 75017 Paris, France. [⊥]Present address: Nanomedicine and Nanotoxicology Laboratory, IFSC, University of São Paulo, P.O. Box 369, São Carlos, SP, 13566-970, Brazil.

ABSTRACT We report *in situ* Raman scattering experiments on single-layer graphene (SLG) and Bernal bilayer graphene (BLG) during exposure to rubidium vapor. The G- and 2D-band evolutions with doping time are presented and analyzed. On SLG, the extended doping range scanned (up to about 10^{14} electrons/cm^2) allows the observation of three regimes in the evolution of the G-band frequency: a continuous upshift followed by a plateau and a downshift. Overall the measured evolution is interpreted as the signature of the competition between dynamic and adiabatic effects upon n-doping. Comparison of the obtained results with theoretical predictions indicates however that a substrate pinning effect occurs and inhibits charge-induced lattice expansion of SLG. At low doping, a direct link between electrostatic gating and Rb doping results is presented. For BLG, the added electrons are shown to be first confined in the top layer, but the system evolves with time toward a more symmetric repartition of the added electrons in both layers. The results obtained on BLG also confirm that the slope of the phonon dispersion close to the K point tends to be slightly reduced at low doping but suggest the occurrence of an unexpected increase of the phonon dispersion slope at higher electron concentration.

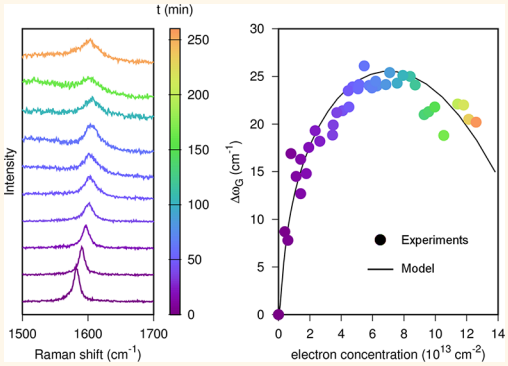

KEYWORDS: graphene · bilayer graphene · alkali · Raman spectroscopy · doping · Rb · charge transfer

Graphene, the latest carbon allotrope to be discovered, is a single layer of carbon atoms arranged in a hexagonal network.[1−4] Stacking a number of graphene layers on top of each other leads to new physical systems: the multilayer graphene, exhibiting different properties than both single-layer graphene (SLG) and graphite. Bernal bilayer graphene (BLG), consisting of the AB stacking of two graphene layers, is the prototype structure of this series. Unlike SLG, where electrons disperse linearly as massless Dirac fermions, BLG has two conduction and valence bands separated by an interlayer coupling energy close to 0.4 eV.[5,6]

Raman spectroscopy provides a convenient tool to characterize graphene samples.[7−9] Especially, it can distinguish between SLG and BLG. On the other hand, Raman spectroscopy is highly sensitive to the electronic structure of these materials and can probe the changes of these properties under external parameters such as doping, chemical modifications, or strain.[10−17] The important features observed in the Raman spectra of all graphene-based materials are the G band and the 2D band (also known as the G′ band).

G and 2D bands are symmetry allowed. The first-order Raman-active G band, located around 1580 cm^{-1}, corresponds to the E_{2g} phonon of graphite at the Brillouin zone center Γ. The 2D band involves two phonons located near the K point. It is associated with a double resonance process, the energy of the phonons depending on the excitation energy.

Both G and 2D bands are sensitive to doping, which is an efficient way to modify the electronic properties of graphene-based materials[18] and to probe electron−phonon interactions in these systems.[10−15,19−21] n-Type doping is of particular interest since on this side adiabatic contributions tend to downshift the G band, while nonadiabatic

* Address correspondence to Ahmed-Azmi.Zahab@univ-montp2.fr.

Received for review August 2, 2012 and accepted November 29, 2012.

Published online November 29, 2012
10.1021/nn3048878

effects result in an upshift of the G band. An inversion in the variation of the G-band frequency is thus expected, which would allow following the interplay between Kohn anomaly removal, charge transfer, and charge-induced lattice expansion in graphene.[19]

Doping can be tuned by means of the electric field effect (electrostatic back- or top-gating doping, in which electric charges are induced by capacitive coupling).[10−14,22] Most of the Raman experiments on doped graphene-based materials have been performed using this method of doping. In the case of back-gating experiments, the maximum Fermi energy shift is limited to about 300 meV, corresponding to a charge density below 10^{13} charge·cm^{-2}. The highest doping can be achieved using a high-capacitance ion-gel gate dielectric (charge density reaches 6×10^{13} charges·cm^{-2}), corresponding to a shift of the Fermi energy of about 800 meV.[22]

Electrochemical doping is another way to dope graphene samples.[23] The charge is mediated by an ohmic contact to the sample and compensated by an electrolyte counterion. However, because the electrochemical setup brings specific requirements (cell geometry, quality of electrodes, purity of chemicals), these experiments are more difficult to carry out than the ones using electrostatic doping. They provide a doping range comparable to the one using a high-capacitance ion-gel gate dielectric.

Charge transfer through adsorption of molecular species is an alternative route to achieve graphene doping.[24] SLG doping with organic molecules,[25−29] sulfuric acid,[30] NO_2,[31] $FeCl_3$,[32,33] halogens,[34] and alkali[35,36] has been recently studied by Raman spectroscopy. Doping of graphene by exposure to alkali (K, Rb) vapors is the most efficient method to achieve high-level n-type doping.[35,36] These previous experimental studies performed *ex situ* focused mainly on heavily n-doped samples and specifically showed that few (1 to 4)-layer graphene samples exhibit profoundly different Raman signatures than thicker graphene or bulk graphite.[35,36] Stage 1 alkali metal intercalated graphites such as KC_8 and RbC_8, corresponding to an energy shift of 1.35 and 1.6 eV (charge density close to 5×10^{14} electrons·cm^{-2}), have been prepared by this way.[24] This extreme electron doping produces major changes in graphite electronic and optical properties. Especially, superconductivity was observed in stage 1 alkali metal intercalated graphites with a superconducting critical transition temperature, T_c, below 1 K (0.55 K for KC_8).[37] The transition temperature reaches 11.5 K for CaC_6.[38] Recently, it was found theoretically that, depending on the doping species, the superconducting transition temperature, T_c, can be higher in monolayer graphene than in the intercalated graphite for the same stochiometry: for LiC_6, T_c is predicted to be close to 8.1 K in graphene *versus* 0.9 K in graphite bulk.[39] All these results underline the interest in preparing graphene samples at high doping levels in order to revisit the understanding of the properties of stage 1 intercalated graphites.[40]

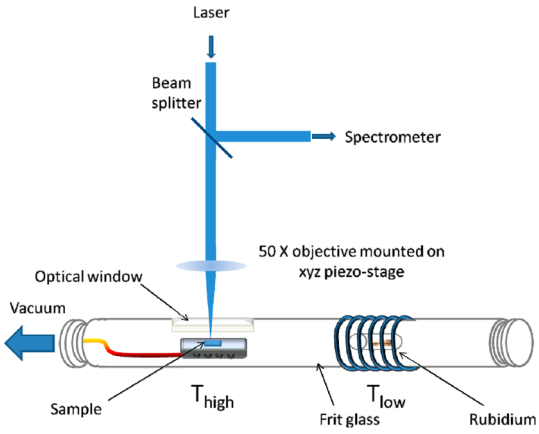

Figure 1. Scheme of the doping reactor. The temperature of both sample and rubidium can be tuned independently to fix the temperature gradient and prevent alkali condensation on the sample. The two chambers are separated by a glass frit to reduce the alkali diffusion flow.

In this paper, we study the n-doping during exposure to rubidium (Rb) vapor of single-layer and Bernal bilayer graphene. We followed *in situ* the evolution of their Raman spectra with doping time. The results presented here complement those obtained by other methods in two different aspects: (i) the n-doping range scanned here (from residual doping up to more than 10^{14} electrons/cm^2 for SLG) extends the one covered by electrostatic and electrochemical methods, (ii) they enable us to make the link between the data obtained at high doping level but for a limited or discrete number of doping values and the one obtained at relatively low doping level but for a quasi-continuous range. Moreover, the broader doping range attainable through alkali doping is used to discuss theoretical predictions of the evolution of the Raman mode frequency as a function of electron concentration.

RESULTS AND DISCUSSION

Figure 1 shows a schematic of the homemade experimental setup used for *in situ* Raman measurements during Rb doping of graphene. The reactor is an adaptation of the two-zone vapor transport method used to produce graphite intercalation compounds.[24] On part of the quartz tube, the sample is fixed close to a heating resistance and maintained at a temperature T_{high}. In front of the sample, a piece of Rb initially sealed in a glass tube under vacuum is inserted in the reactor. Its temperature (T_{low}) can be independently controlled with a resistance heater wrapped around the reactor. Since Rb is in large excess, the two zones are separated by a glass frit acting as a Rb flux limitation. An optical window mounted above the sample surface allows optical excitation and collection in a backscattering geometry.

Single-Layer Graphene. *In situ* experiments were conducted on two different samples. For the first (respectively second) sample, Raman spectra were measured using a 488 nm (respectively 514.5 nm) laser line for excitation. Before doping, each sample was heated at $T_{high} \approx 180$ °C for several hours under vacuum. After this thermal treatment and at $T_{high} \approx 180$ °C under vacuum, the G band is measured at 1581−1582 cm^{-1} (fwhm 11 cm^{-1}) for both experiments. By contrast and as expected,[41] the 2D-band frequencies are located at 2680 cm^{-1} (fwhm 35 cm^{-1}) and 2667 cm^{-1} (fwhm 34 cm^{-1}) in the Raman spectrum excited at 488 and 514.5 nm, respectively. The integrated intensity ratio I_{2D}/I_G is found to be sample dependent; that is, it is evaluated at 4.6 and 6.5 in the spectrum measured at 488 and 514.5 nm, respectively. This difference can however not be fully attributed to the variation in excitation wavelength (evaluated to account for 10%) but is rather due to a slight difference in the initial doping state of each sample as observed on pristine graphene samples.[42] Following the work of Basko *et al.*[43] the difference in doping between the two samples is estimated at $(2-3) \times 10^{12}$ charges·cm^{-2}.

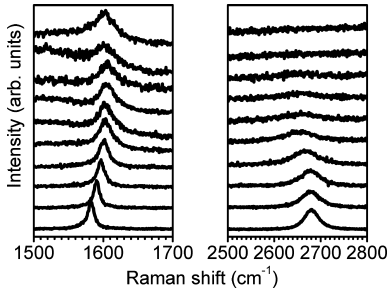

Figure 2. Selected Raman spectra in the G-band (left panel) and 2D-band (right panel) region of SLG recorded with a laser excitation wavelength of 488 nm at different doping times: 0, 4, 19, 39, 47, 53, 62, 105, 164, and 254 min from bottom to top.

Typical Raman spectra recorded *in situ* during rubidium doping are presented in Figure 2. As expected for n-type doping, the G band exhibits first a continuous upshift, which saturates after 1 h of doping. As expected, the 2D band is found to continuously downshift and its relative intensity to decrease.[12,13,22,23] A gradual broadening of the G and 2D peaks upon doping is also noticeable (see Supporting Information) and comparable to that observed in few-layer graphene doped by adsorption or intercalation of Rb.[36]

First, we discuss the G-band frequency evolution, which is plotted in Figure 3a as a function of doping time for the two SLG samples measured at 488 and 514.5 nm. Since the exact starting time of doping is hard to accurately estimate in this kind of experiment, the $t = 0$ time was set by a linear regression of the first points where a G-band upshift is measured. The good agreement between the two data sets shows the reproducibility of the measurements since the G-band frequency does not depend on the excitation wavelength.

As shown in Figure 3a, there is a continuous upshift of the G band during the first doping times, similar to that reported for Raman studies on electrostatically gated graphene.[12,13] Then the G-band frequency saturates at ∼+25 cm^{-1} from its initial frequency. After this plateau a slight downshift (∼−5 cm^{-1}) is observed.

We now examine how our experimental results compare with models in order to estimate the evolution of the charge density of the SLG as a function of time (doping rate) and the maximum level of doping achieved (n_{max}). We started with the theoretical results from ref 19 (red dotted line in Figure 3a), which reproduce well the experimental trend. This model expresses the shift of the G band as the sum of two contributions: an adiabatic one and a nonadiabatic correction. This model is plotted as a dotted line in Figure 3a with the only change being the temperature used for the nonadiabatic correction (450 K as in the

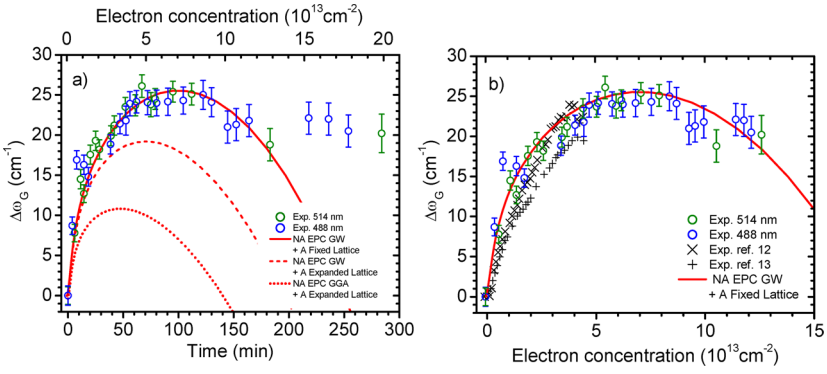

Figure 3. (a) G-band frequency shift as a function of the Rb doping duration measured for two SLG samples with an excitation wavelength of 488 nm (blue dots) and 514.5 nm (green dots), respectively. Red lines correspond to the calculated G-band frequency shift as a function of electron concentration. Red dotted line: Model of Lazzeri *et al.*,[19] which is the sum of an adiabatic (A) contribution and a nonadiabatic (NA) correction. The NA correction has been adapted here for the experimental temperature of 450 K. Red dashed line: Same model except for the NA contribution where the GW evaluation of the EPC has been taken from Lazzeri *et al.*[44] Red line: Same model as red dashed line but keeping the lattice parameter fixed for the A contribution. (b) Experimental data as a function of electron concentration converted from doping time using eq 1 (see text) to fit the adapted model (red line) and compared with experimental results from Das *et al.*[12,13] (black crosses).

experiment instead of 300 K in ref 19); this change is however almost invisible on the Figure 3a scale. The maximum G-band shift predicted by the model of ref 19 is smaller than the experiment. But the electron−phonon coupling (EPC) evaluated by the GW method is actually higher than that predicted by GGA used in ref 19. Thus, as a crude guess, the EPC value $\langle D^2_\Gamma \rangle$ used in ref 19 has been replaced by the GW evaluation of ref 44, yielding the dashed line of Figure 3a. For both dotted and dashed curves, the graphene lattice was allowed to freely expand. On the contrary, in the experiments shown in Figure 3a the single-layer graphene has been pressed on the substrate. This method has been shown to produce pinned layers.[45] In this case, the adiabatic contribution calculated in ref 19 for a fixed lattice should be used. Together with the nonadiabatic contribution using the GW EPC, it gives the full line of Figure 3a. The maximum G-band shift upon n-doping is now in very good agreement with the experiment, as shown in Figure 3. Even if a full GW calculation is desirable and this agreement might involve some fortuitousness, we think that the main physical effects are well captured by this refined model. This assumption is supported by the comparison of the same model with the results of electrostatic gating experiments from the literature (see Supporting Information).

An overall good correlation between experimental data and the model is then obtained, using a constant doping rate of 7×10^{11} electrons·cm^{-2} per min as shown in Figure 3a. Comparison with the experimental data of Das *et al.*[12,13] leads to a comparable estimation of $(8-10) \times 10^{11}$ electrons·cm^{-2} per min. While the approximation of a constant doping rate seems rather good during the first hour of doping, the last measured points show that the doping level saturates. In order to evaluate the maximum doping level attained in our experiments, we thus attempt to convert the doping time (t) in electron concentration (n) by using the first-order rate equation or the so-called Lagergren equation, giving the relation

$$n(t) = n_{eq}(1 - \exp(-kt)) \quad (1)$$

where n_{eq} is the electron concentration in the SLG at equilibrium and k is the first-order rate constant. Using this relation enables obtaining a good fit of the experimental data with the developed model with $n_{eq} \approx 15 \times 10^{13}$ electrons·cm^{-2} and $\tau = 1/k \approx 140$ min (see Figure 3b). We thus determine an initial doping rate of 1×10^{12} electrons·cm^{-2} per min and that the n_{max} attained is determined as $(12 \pm 2) \times 10^{13}$ electrons·cm^{-2}, which corresponds to a Fermi energy above 1 eV.

We now focus on the evolution of the 2D band. Because its frequency depends on the excitation wavelength, the relative rather than the absolute frequency shift is presented in Figure 4 to enable comparison of measurements at 488 and 514.5 nm. The time scale has been converted in Figure 4 for electron concentration using expression 1, and the parameters were determined using the G band. For both excitation wavelengths, the evolutions of the frequency of the 2D band are similar. The frequency continuously decreases by about 40 cm^{-1} until the band disappears completely at $t \approx 1$ h (respectively ~100 min) at 514.5 nm (respectively 488 nm); see Supporting Information. The adiabatic calculation of the 2D-band displacement as a function of the electron concentration extracted from ref 12 as well as experimental results from refs 12 and 13 are also plotted for comparison in Figure 4. A relatively good agreement is found between experimental data presented here and theoretical calculations from ref 12. This suggests that for phonons measured in the Raman spectra excited at 488 or 514 nm, an adiabatic model is sufficient to describe the main trend of the 2D-band behavior under doping. However, several authors[11,12,46] have observed a small stiffening (+2 cm^{-1}) of the 2D band at low n-doping level (on the order of 10^{13} electrons/cm^2). This stiffening, which is not captured by the adiabatic model, can however not be observed in the present study probably due to the small amplitude of this effect as well as the possible slight fluctuations of the doping rate during the first moments of our experiments.

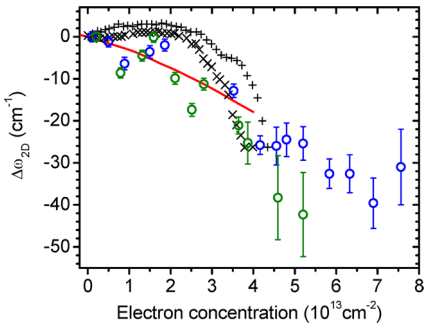

Figure 4. Relative frequency shift of the SLG 2D band as a function of the electron concentration (determined as for Figure 3b) for excitation wavelength of 488 nm (blue open dots) and 514.5 nm (green open dots). The result of the DFT adiabatic calculation (red line) is extracted from ref 12. Black crosses are experimental data measured by electrochemical doping extracted from refs 12 and 13.

In order to address the question of how the results presented here for SLG doping by Rb compare with those of electrostatic gating experiments, we plotted in Figure 5 the relative shift of the 2D band as a function of the relative shift of the G band for both excitation wavelengths. This representation does not suffer from the lack of direct estimation of the doping level and allows a straightforward comparison with the results previously reported by Das *et al.*[12,13] The good agreement between all studies in this time/electron concentration-independent representation confirms the fact that the evolution of G- and 2D-band frequencies of doped SLG is rather insensitive to the way charges are injected. Moreover, this validates the use of alkali

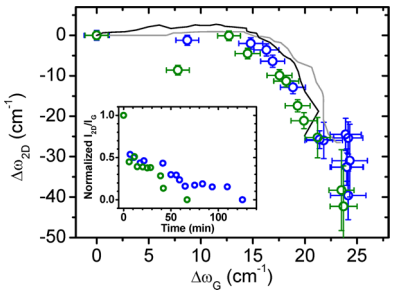

Figure 5. Relative shift of the 2D band as a function of the relative shift of the G band of SLG for excitation wavelengths of 488 nm (blue open dots) and 514.5 nm (green open dots). Black and gray lines are experimental data measured by electrochemical doping extracted from refs 12 and 13. Inset: Normalized integrated intensity ratio of the 2D band and G band (I_{2D}/I_G) as a function of the doping duration for excitation wavelengths of 488 nm (blue open dots) and 514.5 nm (green open dots).

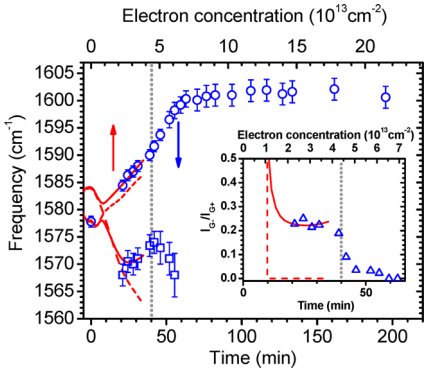

Figure 6. Experimental evolution of the G^+ (blue open dots) and G^- (blue open squares) frequencies of the BLG as a function of the Rb doping duration (bottom *x* axis) for an excitation wavelength of 488 nm. Red lines are theoretical calculations from ref 49 and correspond to the calculated Raman shift in bilayer graphene as a function of electron concentration (top *x* axis). Red full line: Situation 1 where only one layer is doped; the other is neutral. Red dashed line: Situation 2 where both layers are equally charged. The red lines have been downshifted by 3.5 cm^{-1} in order to coincide with the first measured point at $t = 0$. Inset: Ratio between the relative Raman intensities of the lowest (G^-) and the highest (G^+) frequency mode. Blue open triangles are experimental data. Red curves are theoretical calculations from ref 49 corresponding to situations 1 (full line) and 2 (dashed line).

doping to supplement the previous studies conducted by electrostatic or electrochemical doping. In the inset of Figure 5, the normalized intensity ratio I_{2D}/I_G is plotted as a function of the doping duration for both excitation wavelengths. As expected for SLG, the ratio is maximal for neutral graphene and decreases quickly, whereas the electron density increases, as attributed to enhancement of electron−electron collisions.[43] This result is also consistent with electrochemical doping studies.[12,13,23] Moreover, the observation that the 2D signal vanishes earlier in the study conducted at 2.41 eV (514.5 nm) when compared to the one made at 2.54 eV (488 nm) qualitatively agrees with the fact that blockage of the resonant Raman pathways will occur when the Fermi energy reaches $E_{Laser}/2 - \hbar\omega_D$.[22,43]

Bilayer Graphene. Similar experiments have been performed on a Bernal bilayer graphene sample. The general trends of G and 2D evolutions upon doping are overall similar to those observed for SLG, but several differences are noticeable.

Concerning the G^- mode, it has to be reminded that the E_{2g} phonon mode of SLG gives rise to two modes, at the center of the Brillouin zone, for BLG: a Raman-active symmetric mode (E_g symmetry: in-phase displacements of the atoms in the two layers) and a non-Raman-active antisymmetric mode (E_u symmetry: out-of-phase displacements of the atoms in the two layers).[47−51] In our experiments, a splitting of the G band within the first hour of doping in two modes, G^+ and G^-, is observed (see Supporting Information Figures S4 and S5). The splitting of the G band in two components has already been observed in doped BLG.[6,33,48−53] This splitting is understood by considering that the doping levels of both layers are not equivalent, leading to breaking of the inversion symmetry of BLG.[6,48−52] Consequently, the symmetric E_g and antisymmetric E_u modes are mixed and the two new eigen-modes are Raman active.[6,48−52] The evolution of the G^+ and G^- positions as a function of the doping duration is presented in Figure 6. The G^+ mode shows, as for SLG, a continuous upshift up to about +25 cm^{-1} during the first hour of doping followed by a plateau. At the lowest doping level for which the measurement of the G^- mode is possible, it is located at ∼16−17 cm^{-1} below G^+. For a doping time between 20 and 40 min, it upshifts in a similar manner as the G^+ mode. Between $t = 40$ min and $t = 55$ min, the G^- mode downshifts and it vanishes after one hour of doping. As shown in the inset of Figure 6, the integrated intensity ratio (I_{G-}/I_{G+}) is first constant around 0.2 (for *t* between 20 and 40 min) and decreases to reach 0 (corresponding to a complete disappearance of the G^- component) at $t = 1$ h. In Figure 6, a comparison of our data with the theoretical predictions of Gava *et al.*,[49] performed by considering that only one layer is charged and the second stays neutral (situation 1), is presented (Figure 6, solid red lines). For $t < 40$ min, good agreement is found for both the frequency evolutions and the I_{G-}/I_{G+} ratio by using a supposed constant doping rate of $\sim 11 \times 10^{11}$ electrons·cm^{-2} per min. This conversion factor is very close (10% higher) to the one determined for SLG. In Figure 6, we also plotted as dotted red lines the theoretical predictions of Gava *et al.*[49] corresponding to situation 2, where both layers are equally charged. In this case, G^- is not Raman active, and thus $I_{G-}/I_{G+} = 0$. Moreover, the frequency of the non-Raman-active G^- mode is predicted to be lower than in situation 1 for $n > 2 \times 10^{13}$ electrons·cm^{-2}. Consequently, we interpret the behavior change occurring at $t \approx 40$ min as an evolution of the system from situation 1 to

situation 2. In summary, our results suggest that the doping of one layer (the top layer) is faster than the other one (the bottom layer) within the first ~40 min and that the system evolves toward a more symmetric situation attained at $t \approx 1$ h. It should however be noted that the disorder-induced broadening observed in our experiment can influence in particular G^- frequency evolution upon doping[6] and will have to be taken into account to describe more accurately the observed evolutions.

As in the case of SLG, the results obtained on BLG show strong indications that the doping rate has dramatically decreased after 1 h 30 min of doping. No extensive theoretical predictions or experimental data on a broad doping range are however available in the literature for BLG. For this reason and because of the observed change of charge repartition among the two layers during the experiment, it appears highly speculative to conduct the same analysis on the evolution of the doping rate with time as it has been done for SLG. Despite that, the maximum electron concentration attained can be roughly estimated at $(9 \pm 3) \times 10^{13}$ electrons·cm^{-2}, corresponding to a Fermi energy of 0.7 ± 0.2 eV.

The investigation of the 2D band of BLG is of particular interest to study the evolution of the phonon dispersion close to the K point under doping. Indeed, the profile of the 2D-band presents four components, corresponding to four processes. In each of these processes, a peculiar phonon wavevector is photoselected at a single excitation wavelength.[7] Due to the dispersion of the electronic dispersion curves, the component of lowest frequency corresponds to the shortest wavevector, whereas the higher frequency corresponds to the largest wavevector. Because the two components corresponding to the intermediate wavevectors have much stronger intensities compared to the components assigned to the shortest and highest wavevectors, we choose to fit the 2D band for each doping level with two Lorentzian functions ($2D_A$ and $2D_B$) following the same procedure as Das *et al.*[13] In our case (excitation at 2.54 eV), the phonon wavevectors associated with each one of these components are $q_A \approx 0.16(2\pi/a)$ and $q_B \approx 0.11(2\pi/a)$, where a is the lattice parameter of graphene. These wavevectors correspond, in the case of the SLG 2D band, to phonons photoselected with blue and red excitation, respectively. In other words, since separation of the components of the BLG 2D band reflects the phonon dispersion, the doping of BLG allows following the evolution of the phonon dispersion slope close to the K point using a single excitation wavelength.[54] In Figure 7 is presented the frequency evolution of each of the two components ω_{2DA} and ω_{2DB} as a function of doping duration. On one hand, the overall trends look similar for both components $2D_A$ and $2D_B$: a moderate or no downshift is first observed until $t \approx 40$ min; the downshift with time is then more pronounced until $t \approx 1$ h, after which no more evolution is measured. On the other hand, the separation $(\omega_{2DA} - \omega_{2DB})$ is found to change. It shows first a slight decrease to reach 80% of its initial value at $t = 31$ min, followed by a progressive increase to reach and stay at about twice its initial value after $t \approx 1$ h. The first regime could reflect a decrease of the slope of the phonon dispersion close to the K point upon doping as predicted theoretically for SLG by DFT in the GW approximation[20] or by DFT-based nonorthogonal tight binding[21] and recently observed experimentally for BLG.[54] It should be noticed that the doping method used in ref 54, which was demonstrated to induce a confinement of 85% of the charges in the top layer,[53] shows similarities with the situation observed here for $t < 40$ min. The progressive increase of the separation between ω_{2DA} and ω_{2DB} observed for $t > 31$ min could correspondingly reflect an increase in the slope of the phonons' dispersion. Although such an increase is unexpected theoretically,[20] an extraction of the experimental data from ref 13 shows that an increase of 20% of the separation $(\omega_{2DA} - \omega_{2DB})$ has also been observed for a charge density of 4.5×10^{13} electrons·cm^{-2} by electrochemical doping of BLG, in the case where both layers are equivalently charged.[13] Overall, this analysis raises two open questions: Is the evolution of the frequency separation between the 2D-band components of BLG affected by the charge repartition between the layers at low doping? What is the origin of the increase of the separation $(\omega_{2DA} - \omega_{2DB})$ at high doping? Further experimental and theoretical works are needed to answer these questions.

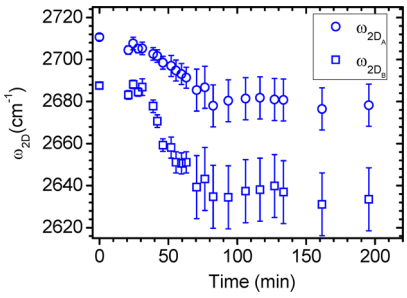

Figure 7. Evolution of the frequency of the two fitted components of the BLG 2D band as a function of the doping duration.

CONCLUSION

An *in situ* Raman monitoring of SLG and BLG doping upon Rb vapor exposure has been presented, and the time evolutions of both G and 2D bands have been analyzed.

For SLG, the frequency and the intensity ratio of the two main Raman features (G and 2D bands) were found to behave in a similar manner as compared to electrochemical doping experiments[12,13] on the overlapping doping range. The broader n-doping range scanned

here allows the observation of three regimes in the evolution of the G-band frequency, which are related to the competition between nonadiabatic effects and adiabatic contributions. A quantitative agreement is found between the measured G-band shift as a function of electron concentration and an adapted model based on the theoretical work of Lazzeri *et al.*[19] This adapted model is simply derived by replacing the GGA EPC value by the one evaluated by the GW method[44] and considering that the lattice of the SLG pressed on the Si/SiO_2 substrate is not allowed to expand.[19,45] This hypothesis deserves to be tested, for example, by conducting doping experiments on suspended graphene. Concerning the evolution of the 2D-band frequency upon doping, an adiabatic model was found to be sufficient to describe the main trend observed. Finally, we confirm that alkali doping allows reaching n-doping levels inaccessible by other techniques and evaluate that the maximum electron concentration attained here is $\sim 12 \times 10^{13}$ electrons$\cdot$cm^{-2} (*i.e.*, $E_F \approx 1$ eV).

On BLG, analysis of the G-band profile evolution allowed us to follow the time evolution of the charge repartition among the two layers. A G-band splitting in the two components G^+ and G^- has been evidenced on BLG for early doping times. The G^- component was also shown to vanish for longer doping times. We conclude that at first only the top layer is doped, but the system gradually evolves with time toward a more symmetric repartition of the added electrons in both layers. Bilayer graphene also offers interesting perspectives since it allows following the evolution of the slope of phonon dispersion close to the K point using a single excitation wavelength. The results obtained here confirm that the phonon dispersion slope close to the K point tends to be slightly reduced[20,21,54] at low doping (typically below 4×10^{13} electrons$\cdot$cm^{-2}). By contrast, the separation between the two main components of the BLG 2D band was found to increase at higher electron concentration, suggesting the occurrence of an unexpected increase of the phonon dispersion slope upon doping.

METHODS

Sample Preparation. The graphene samples are prepared by micromechanical cleavage of bulk highly ordered pyrolytic graphite and deposited on a silicon wafer covered with 90 nm SiO_2. The number of layers is determined by optical contrast and Raman spectroscopy.[55] The absence of the D band shows on one hand the good crystalline quality of the sample and on the other hand a large enough sample size to avoid edge effects.

Doping Protocol. The reactor is first outgased ($P \approx 10^{-6}$ mbar) and the sample heated at $T_{high} \approx 180$ °C for several hours under vacuum. Then the rubidium container is broken, and vapor phase doping under dynamical vacuum is started by increasing T_{low} up to ~160 °C for about 1 min. T_{low} is then decreased and maintained at ~150 °C in order to achieve a steady state with a constant Rb partial pressure and to keep a temperature gradient of ~30 °C to achieve a slow doping rate compatible with *in situ* Raman measurements and to prevent alkali-metal condensation on the sample.[56]

Raman Spectroscopy. Raman spectra were recorded approximately every 5 min during the whole experiment (the acquisition time was 1 min for each spectrum) with blue line 488 nm (2.54 eV) or green line 514 nm (2.41 eV) of an Ar/Kr mixed gas laser as excitation and using an iHR550 Jobin-Yvon spectrometer (grating 1800 grooves/mm, precision $\sim \pm 1$ cm^{-1}) in a micro Raman backscattering configuration. The homemade microscope is equipped with a 50× objective (N.A. 0.5, W.D. 11 mm) mounted on a three-axis piezoelectric stage (PIMars P-563 PI) to ensure the precise positioning and focusing of the laser spot without moving the reactor. The power density impinging on the sample is kept around 0.5 mW/μm^2 to avoid additional heating of the sample or laser-assisted Rb desorption.

Conflict of Interest: The authors declare no competing financial interest.

Supporting Information Available: Evolution of the full width at half-maximum of SLG G and 2D bands with doping time. Comparison of the adapted model with experimental data from the literature. SLG 2D-band relative frequency shift as a function of time. Raman spectra of BLG G and 2D bands measured *in situ* during Rb doping. Raman spectrum of BLG showing the splitting of the G band. This material is available free of charge *via* the Internet at http://pubs.acs.org.

Acknowledgment. We thank R. Aznar for technical support and V. N. Popov, F. Mauri, and M. Kalbac for useful discussions. This work has been done in the framework of the GDRI GNT No 3217 "Graphene and Nanotubes: Sciences and Application". The authors acknowledge financial support from ANR Grafonics. D.N. acknowledges funding from CNRS.

REFERENCES AND NOTES

1. Novoselov, K. S.; Geim, A. K.; Morozov, S. V.; Jiang, D.; Zhang, Y.; Dubonos, S. V.; Grigorieva, I. V.; Firsov, A. A. Electric Field Effect in Atomically Thin Carbon Films. *Science* **2004**, *306*, 666–669.
2. Novoselov, K. S.; Geim, A. K.; Morozov, S. V.; Jiang, D. M.; Katsnelson, I.; Grigorieva, I. V.; Dubonos, S. V.; Firsov, A. A. Two-Dimensional Gas of Massless Dirac Fermions in Graphene. *Nature* **2005**, *438*, 197–200.
3. Zhang, Y.; Tan, Y.-W.; Stormer, H. L.; Kim, P. Experimental Observation of the Quantum Hall Effect and Berry's Phase in Graphene. *Nature* **2005**, *438*, 201–204.
4. Novoselov, K. S.; Geim, A. K. The Rise of Graphene. *Nat. Mater.* **2007**, *6*, 183–191.
5. McCann, E. C.; Falko, V. I. Landau-Level Degeneracy and Quantum Hall Effect in a Graphite Bilayer. *Phys. Rev. Lett.* **2006**, *96*, 086805.
6. Ando, T. Anomaly of Optical Phonons in Bilayer Graphene. *J. Phys. Soc. Jpn.* **2006**, *76*, 104711.
7. Ferrari, A. C.; Meyer, J. C.; Scardaci, V.; Casiraghi, C.; Lazzeri, M.; Mauri, F.; Piscanec, S.; Jiang, D.; Novoselov, K. S.; Roth, S.; *et al.* Raman Spectrum of Graphene and Graphene Layers. *Phys. Rev. Lett.* **2006**, *97*, 187401.
8. Mafra, D. L.; Malard, L. M.; Doorn, S. K.; Htoon, Han; Nilsson, J.; Castro Neto, A. H.; Pimenta, M. A. Observation of the Kohn Anomaly near the K Point of Bilayer Graphene. *Phys. Rev. B* **2009**, *80*, 241414.
9. Berciaud, S.; Ryu, S.; Brus, L. E.; Heinz, T. F. Probing the Intrinsic Properties of Exfoliated Graphene: Raman Spectroscopy of Free-Standing Monolayers. *Nano Lett.* **2009**, *9*, 346–352.
10. Pisana, S.; Lazzeri, M.; Casiraghi, C.; Novoselov, K. S.; Geim, A. K.; Ferrari, A. C.; Mauri, F. Breakdown of the Adiabatic Born-Oppenheimer Approximation in Graphene. *Nat. Mater.* **2007**, *6*, 198–201.

11. Yan, J.; Zhang, Y.; Kim, P.; Pinczuk, A. Electric Field Effect Tuning of Electron-Phonon Coupling in Graphene. *Phys. Rev. Lett.* **2007**, *98*, 166802.
12. Das, A.; Pisana, S.; Chakraborty, B.; Piscanec, S.; Saha, S. K.; Waghmare, U. V.; Novoselov, K. S.; Krishnamurthy, H. R.; Geim, A. K.; Ferrari, A. C.; *et al*. Monitoring Dopants by Raman Scattering in an Electrochemically Top-Gated Graphene Transistor. *Nat. Nanotechnol.* **2008**, *3*, 210–215.
13. Das, A.; Chakraborty, B.; Piscanec, S.; Pisana, S.; Sood, A. K.; Ferrari, A. C. Phonon Renormalization in Doped Bilayer Graphene. *Phys. Rev. B* **2009**, *79*, 155417.
14. Malard, L. M.; Nilsson, J.; Elias, D. C.; Brant, J. C.; Plentz, F.; Alves, E. S.; Castro Neto, A. H.; Pimenta, M. A. Probing the Electronic Structure of Bilayer Graphene by Raman Scattering. *Phys. Rev. B* **2007**, *76*, 201401.
15. Alzina, F.; Tao, H.; Moser, J.; Garcia, Y.; Bachtold, A.; Sotomayor-Torres, C. M. Probing the Electron-Phonon Coupling in Ozone-Doped Graphene by Raman Spectroscopy. *Phys. Rev. B* **2010**, *82*, 075422.
16. Mohiuddin, T. M. G.; Lombardo, A.; Nair, R. R.; Bonetti, A.; Savini, G.; Jalil, R.; Bonini, N.; Basko, D. M.; Galiotis, C.; Marzari, N.; *et al*. Uniaxial Strain in Graphene by Raman Spectroscopy: G Peak Splitting, Gruneisen Parameters, and Sample Orientation. *Phys. Rev. B* **2009**, *79*, 205433.
17. Yoon, D.; Son, Y.-W.; Cheong, H. Strain-Dependent Splitting of the Double-Resonance Raman Scattering Band in Graphene. *Phys. Rev. Lett.* **2011**, *106*, 155502.
18. Botswick, A.; Ohta, T.; Seyller, T.; Horn, K.; Rotenberg, E. Quasiparticle Dynanmics in Graphene. *Nat. Phys.* **2007**, *3*, 36–40.
19. Lazzeri, M.; Mauri, F. Nonadiabatic Kohn Anomaly in a Doped Graphene Monolayer. *Phys. Rev. Lett.* **2006**, *97*, 266407.
20. Attaccalite, C.; Wirtz, L.; Lazzeri, M.; Mauri, F.; Rubio, A. Doped Graphene as Tunable Electron-Phonon Coupling Material. *Nano Lett.* **2010**, *10*, 1172–1176.
21. Popov, V. N.; Lambin, P. Dynamic and Charge Doping Effects on the Phonon Dispersion of Graphene. *Phys. Rev. B* **2010**, *82*, 045406.
22. Chen, C.-F.; Park, C.-H.; Boudouris, B. W.; Horng, J.; Geng, B.; Girit, C.; Zettl, A.; Crommie, M. F.; Segalman, R. A.; Louie, S. G.; *et al*. Controlling iInelastic Light Scattering Quantum Pathways in Graphene. *Nature* **2011**, *471*, 617–620.
23. Kalbac, M.; Reina-Cecco, A.; Farhat, H.; Kong, J.; Kavan, L.; Dresselhaus, M. S. The Influence of Strong Electron and Hole Doping on the Raman Intensity of Chemical Vapor-Deposition Graphene. *ACS Nano* **2010**, *4*, 6055–6063.
24. Dresselhaus, M. S.; Dresselhaus, G. Intercalation Compounds of Graphite. *Adv. Phys.* **1981**, *30*, 139.
25. Zhang, Z.; Huang, H.; Yang, X.; Zang, L. Tailoring Electronic Properties of Graphene by π-π Stacking with Aromatic Molecules. *J. Phys. Chem. C Lett.* **2011**, *2*, 2897–2905, and references therein.
26. Medina, H.; Lin, Y.-C.; Obergfell, D.; Chiu, P.-C. Tuning of Charge Densities in Graphene by Molecule Doping. *Adv. Funct. Mater.* **2011**, *21*, 2687–2692.
27. Late, D. J.; Ghosh, A.; Chakraborty, B.; Sood, A. K.; Waghmare, U. V.; Rao, C. N. R. Molecular Charge-Transfer Interaction with Single-Layer Graphene. *J. Exp. Nanosci.* **2011**, *6*, 641–651.
28. Peimyoo, W.; Yu, T.; Shang, J.; Cong, C.; Yang, H. Thickness-Dependent Azobenzene Doping in Mono- and Few-Layer Graphene. *Carbon* **2012**, *50*, 201–208.
29. Singh, A. K.; Iqbal, M. W.; Singh, V. K.; Iqbal, M. Z.; Lee, J. H.; Chun, S.-H.; Shin, K.; Eom, J. Molecular n-Doping of Chemical Vapor Deposition Grown Graphene. *J. Mater. Chem.* **2012**, *22*, 15168.
30. Zhao, W. J.; Tan, P. H.; Zhang, J.; Liu, J. A. Charge Transfer and Optical Phonon Mixing in Few-Layer Graphene Chemically Doped with Sulfuric Acid. *Phys. Rev. B* **2010**, *82*, 245423.
31. Crowther, A. C.; Ghassaei, A.; Jung, N.; Brus, L. E. Strong Charge-Transfer Doping of 1 to 10 Layer Graphene by NO_2. *ACS Nano* **2012**, *6*, 1865–1875.
32. Zhan, D.; Sun, L.; Ni, Z. H.; Liu, L.; Fan, X. F.; Wang, Y. Y.; Yu, T.; Lam, Y. M.; Huang, W.; Shen, Z. X. $FeCl_3$-Based Few-Layer Graphene Intercalation Compounds: Single Linear Dispersion Electronic Band Structure and Strong Charge Transfer Doping. *Adv. Funct. Mater.* **2010**, *20*, 3504–3509.
33. Zhao, W.; Tan, P. H.; Liu, J.; Ferrari, A. C. Intercalation of Few-Layer Graphite Flakes with $FeCl_3$: Raman Determination of Fermi Level, Layer by Layer Decoupling, and Stability. *J. Am. Chem. Soc.* **2011**, *133*, 5941–5946.
34. Jung, N.; Kim, N.; Jockusch, S.; Turro, N. J.; Kim, P.; Brus, L. Charge Transfer Chemical Doping of Few Layer Graphenes: Charge Distribution and Band Gap Formation. *Nano Lett.* **2009**, *9*, 4133–4137.
35. Howard, C. A.; Dean, M. P. M.; Withers, F. Phonons in Potassium-Doped Graphene: the Effects of Electron-Phonon Interactions, Dimensionality, and Adatom Ordering. *Phys. Rev. B* **2011**, *84*, 241404.
36. Jung, N.; Kim, B.; Crowther, A. C.; Kim, N.; Nuckolls, C.; Brus, L. Optical Reflectivity and Raman Scattering in Few-Layer-Thick Graphene Highly Doped by K and Rb. *ACS Nano* **2011**, *5*, 5708–5716.
37. Hannay, N. B.; Geballe, T. H.; Matthias, B. T.; Andres, K.; Schmidt, P.; MacNair, D. Superconductivity in Graphitic Compounds. *Phys. Rev. Lett.* **1965**, *14*, 225.
38. Emery, N.; Herold, C.; d'Astuto, M.; Garcia, V.; Bellin, Ch.; Mareche, J. F.; Lagrange, P.; Loupias, G. Superconductivity of Bulk CaC_6. *Phys. Rev. Lett.* **2005**, *95*, 087003.
39. Profeta, G.; Calandra, M.; Mauri, F. Phonon-Mediated Superconductivity in Graphene by Lithium Deposition. *Nat. Phys.* **2012**, *8*, 131–134.
40. Chacón-Torres, J. C.; Ganin, A. Y.; Rosseinsky, M. J.; Pichler, T. Raman Response of Stage-1 Graphite Intercalation Compounds Revisited. *arXiv* **2012**, 1204.5971v3.
41. Malard, L. M.; Pimenta, M. A.; Dresselhaus, G.; Dresselhaus, M. S. Raman Spectroscopy in Graphene. *Phys. Rep.* **2009**, *473*, 51–87.
42. Casiraghi, C. Doping Dependence of the Raman Peaks Intensity of Graphene Close to the Dirac Point. *Phys. Rev. B* **2009**, *80*, 233407.
43. Basko, D. M.; Piscanec, S.; Ferrari, A. C. Electron-Electron Interactions and Doping Dependence of the Two-Phonon Raman Intensity in Graphene. *Phys. Rev. B* **2009**, *80*, 165413.
44. Lazzeri, M.; Attaccalite, C.; Wirtz, L.; Mauri, F. Impact of the Electron-Electron Correlation on Phonon Dispersion: Failure of LDA and GGA DFT Functionals in Graphene and Graphite. *Phys. Rev. B* **2008**, *78*, 081406.
45. Ferralis, N.; Maboudian, R.; Carraro, C. Determination of Substrate Pinning in Epitaxial and Supported Graphene Layers *via* Raman Scattering. *Phys. Rev. B* **2011**, *83*, 081410(R).
46. Stampfer, C.; Molitor, F.; Graf, D.; Ensslin, K.; Jungen, A.; Hierold, C.; Wirtz, L. Raman Imaging of Doping Domains in Graphene on SiO_2. *Appl. Phys. Lett.* **2007**, *91*, 241907.
47. Malard, L. M.; Guimaraes, M. H. D.; Mafra, D. L.; Mazzoni, M. S. C.; Jorio, A. Group-Theory Analysis of Electrons and Phonons in N-Layer Graphene Systems. *Phys. Rev. B* **2009**, *79*, 125426.
48. Malard, L. M.; Elias, D. C.; Alves, E. S.; Pimenta, M. A. Observation of Distinct Electron-Phonon Couplings in Gated Bilayer Graphene. *Phys. Rev. Lett.* **2008**, *101*, 25740.
49. Gava, P.; Lazzeri, M.; Saitta, A. M.; Mauri, F. Probing the Electrostatic Environment of Bilayer Graphene Using Raman Spectra. *Phys. Rev. B* **2009**, *80*, 155422.
50. Yan, J.; Villarson, T.; Henriksen, E. A.; Kim, P.; Pinczuk, A. Optical Phonon Mixing in Bilayer Graphene with a Broken Inversion Symmetry. *Phys. Rev. B* **2009**, *80*, 241417.
51. Mafra, D. L.; Gava, P.; Malard, L. M.; Borges, R. S.; Silva, G. G.; Leon, J. A.; Plentz, F.; Mauri, F.; Pimenta, M. A. Characterizing Intrinsic Charges in Top Gated Bilayer Graphene Device by Raman Spectroscopy. *Carbon* **2012**, *50*, 3435–3439.
52. Ando, T.; Koshino, M. Field Effects on Optical Phonons in Bilayer Graphene. *J. Phys. Soc. Jpn.* **2009**, *78*), 034709.
53. Bruna, M.; Borini, S. Observation of Raman G-Band Splitting in Top-Doped Few-Layer Graphene. *Phys. Rev. B* **2010**, *81*, 125421.

54. Bruna, M.; Borini, S. Raman Signature of Electron-Electron Correlation in Chemically Doped Few-Layer Graphene. *Phys. Rev. B* **2011**, *83*, 241401.
55. Yoon, D.; Moon, H.; Son, Y.; Choi, J.; Park, B.; Cha, Y.; Kim, Y.; Cheong, H. Interference Effect on Raman Spectrum of Graphene on SiO_2/Si. *Phys. Rev. B* **2009**, *80*, 125422.
56. Bendiab, N.; Spina, L.; Zahab, A.; Poncharal, P.; Marlière, C.; Bantignies, J. L.; Anglaret, E.; Sauvajol, J. L. Combined *in Situ* Conductivity and Raman Studies of Rubidium Doping of Single-Wall Carbon Nanotubes. *Phys. Rev. B* **2001**, *63*, 153407.